On the collapse of a post-tensioned reinforced concrete truss bridge during the construction phases

Marco ZUCCA[(2)*], Sergio TATTONI[(1)], Marta DI CASTRI[(1)], Marco SIMONCELLI[(1)]

(1) Department of Architecture, Built Environment and Construction Engineering
Politecnico di Milano, Milano, Italy
(2) Department of Civil, Environmental Engineering and Architecture
University of Cagliari, Italy
* Corresponding author. E-mail: marco.zucca2@unica.it

Abstract

On March 2018 a post-tensioned reinforced concrete (RC) truss bridge, built inside a North American university campus using the Accelerated Bridge Construction (ABC) method, collapsed during the construction phases, while the bars of a diagonal member were being re-tensioned. This process was not part of the scheduled construction phases, but it was decided by the designers after having observed several cracks in the structural nodes.

This paper aims to analyse the final design of the bridge useful to determine the hypothetical causes of the collapse. Several numerical analyses have been performed to reproduce the behaviour of the different structural elements during the construction phases. In particular, construction stage analyses have been carried out to obtain the internal actions acting on the structural elements and on the nodes during the different construction steps and in order to analyse in detail the critical phases where the occurrence of the collapse has been hypothesized. The collapse mechanism is identified in the shear failure of a node of the concrete truss during the re-tensioning of a diagonal element. In fact, the reapplication of the post-tension had increased the axial force of the diagonal and consequently the shear action on the node. Moreover, the results obtained have shown that the bridge has never been in safe conditions, mainly because the interface surface of the cold joints had not undergone any type of work and remained smooth.

Keywords*: reinforced concrete, truss bridge, construction stage analysis, collapse mechanism identification.*

1. Introduction

During last years, the occurrence of different collapses that interested reinforced concrete (RC) bridges, have focused the attention of the scientific community and the designers, on the correct evaluation of the causes that led to these unwanted events. The most important causes that led the failure of different bridges have been discussed by different Authors. Deng et al. [1] have divided the factors which bring to the collapse of bridges into two broad categories: (i) natural factors (flood, scour, earthquake, landslide, debris flow, hurricane, typhoon, wind, etc) and (ii) human factors (imperfect design and construction method, collision, vehicle overloading, fire, terrorist attack, lack of inspection and maintenance, etc.). Some of these causes have been also identified by Zhang et al. [2], which focussed the attention on five main problems: (i) design error, (ii) construction mistakes, (iii) hydraulic, (iv) collision and (v) overload. Xu et al. [3] analysed the collapse of 302 highway bridges occurred in China between 2000 and 2014 due to human (design and construction) mistakes. In Fan et al. [4] the causes that led to the collapse of Yangmingtan Bridge, occurred on 24 August 2012 in Harbin City, have been investigated determining the influence of the truck overload in the failure mechanism. Diaz et al. [5] investigated the main causes which characterized the failure of bridges in Colombia highlighting that: the 36% of the analysed bridge were steel bridges and their failure was related to structural deficiencies while the other 64% were concrete bridges, where the causes of the collapse were attributable to overloads. Analysing the causes which led to the failure of RC bridges, the collapse occurs during the construction process appears to be among the most frequent [6-12]. In fact, considering the constant evolution of architectural design which has led to the realization of more and more complex structures, the construction phases require increasingly greater efforts [13-15]. Among this wide range of structures, post-tensioned RC truss bridges stand out for their technical complexity.

Some Authors proposed different strategies to evaluate the collapse mechanism of a bridge. Crespi et al. [16] proposed an efficient procedure to evaluate the collapse mechanisms of existing RC bridges under horizontal loads, focusing attention on seismic action, introducing a simplified approach to account the influence of corrosion effects due to carbonation on the load-bearing capacity of the bridges. Domenaschi et al. [17] reproduced the failure mechanism of the well-known Polcevara viaduct (built in Italy) by using the applied element method, showing the exact match between numerical and the real collapse mechanism. Heng et al. [18] proposed an advanced finite element model to simulate the failure of a RC bridge subjected to a heavy truck impact on a pier.

In this paper the failure of a post-tensioned RC truss pedestrian bridge, built inside a North American university campus using the Accelerated Bridge Construction (ABC) method, has been analysed in detail by means several numerical analyses in order to evaluate the causes which led to the initiation of the failure mechanism. In particular, construction stage analysis has been performed to analyse the evolution of the internal actions acting on the different structural elements during the construction process. The results have shown that the collapse mechanism is identified in the interface shear failure of a node during the re-tensioning of the corresponding diagonal truss concrete element. In fact, the reapplication of the post-tension had increased the axial force on the diagonal element and consequently the shear action on the node. Moreover, one of the main problems is related to the underestimation of the forces acting in the truss and to the overestimation of the load-bearing capacity of the related nodes. The analysed bridge has never been in safe conditions, mainly because the interface surface of the cold joints had not undergone any type of work and remained smooth, contrary to what was assumed in the design phase.

2. The post-tensioned RC truss bridge

The analysed post-tensioned RC truss pedestrian bridge having a total length of 81 m, has been designed to be built inside a North American university campus. The bridge was conceived as an "I-like" shape RC beam with the deck as the lower part of the I-beam and the upper part has the function of canopy. Finally, the web of such ideal I-beam, is made by a non-symmetric truss beam (Fig. 1).

Figure 1: The analysed RC truss bridge [19].

The bridge consists of two spans 29 and 52 meters long, respectively. The structural behaviour of the bridge is assimilable to a three simply supported beam while the cables, shown in Fig. 1, have only an aesthetic function. It is important to notice that the inclination of the RC diagonal structural elements follows the cables direction, leading to a non-symmetric truss beam. The deck is made of prestressed reinforced concrete with prestressing acting in both longitudinal and transversal directions while, the canopy, is realized in prestressed reinforced concrete having the prestress action acting only in longitudinal direction. The RC structural elements have been realized using high-performance concrete obtained by introducing silica fume and fly ash in concrete mix design in order to have greater resistance and durability.

The other structural elements which characterize the truss beam are made of reinforced concrete with unbonded post-tensioned cables. Table 1 summarizes the mechanical properties of the used materials.

Table 1: Materials mechanical properties.

concrete Class VI [20]		
Compressive strength (f_c)	58.60	[MPa]
Tensile strength (f_{ct})	4.53	[MPa]
Young modulus (E_c)	32964	[MPa]
Poisson ratio (ν_c)	0.2	[-]
Thermal coefficient (T_c)	$6 \cdot 10^{-6}$	[1/F]
Unit weight (γ_c)	23.5	[kN/m^3]
steel for concrete reinforcement: ASTM A615 Grade 60 [21]		
Average yield strength ($f_{y,60}$)	415	[MPa]
Average ultimate strength ($f_{t,60}$)	620	[MPa]
Young modulus ($E_{s,60}$)	199950	[MPa]
Poisson ratio ($\nu_{s,60}$)	0.3	[-]
Unit weight ($\gamma_{s,60}$)	77.09	[kN/m^3]
steel for post-tensioned rebars ASTM A722 Grade 150 [22]		
Average yield strength ($f_{y,150}$)	827	[MPa]

Average ultimate strength ($f_{t,150}$)	1035	[MPa]
Maximum jacking stress	827.37	[MPa]
Maximum anchoring stress	723.95	[MPa]
After anchor set	723.95	[MPa]
Anchor set	0	[MPa]
Young modulus ($E_{s,150}$)	200000	[MPa]
Poisson ratio ($\nu_{s,150}$)	0.3	[-]
Unit weight ($\gamma_{s,150}$)	77.09	[kN/m^3]
steel for tendons ASTM A416 Grade 270 [23]		
Diameter	15.2	[mm]
Average yield strength ($f_{y,270}$)	1709	[MPa]
Average ultimate strength ($f_{t,270}$)	1923	[MPa]
Maximum jacking stress	1507.80	[MPa]
Maximum anchoring stress away from anchorages	1377.60	[MPa]
After anchor set	1303.10	[MPa]
Friction coefficient	0.23	[-]
Young modulus ($E_{s,270}$)	200000	[MPa]
Poisson ratio ($\nu_{s,270}$)	0.3	[-]
Unit weight ($\gamma_{s,270}$)	77.09	[kN/m^3]

It is important to highlight that ASTM A615 Grade 60 steel has been used for the steel reinforcement while for the post-tensioned rebars and tendons ASTM A722 Grade 150 steel and ASTM A416 Grade 270 steel have been considered, respectively.

As mentioned before, the bridge is characterized by the presence of three RC piers which support the truss beam (Fig. 2).
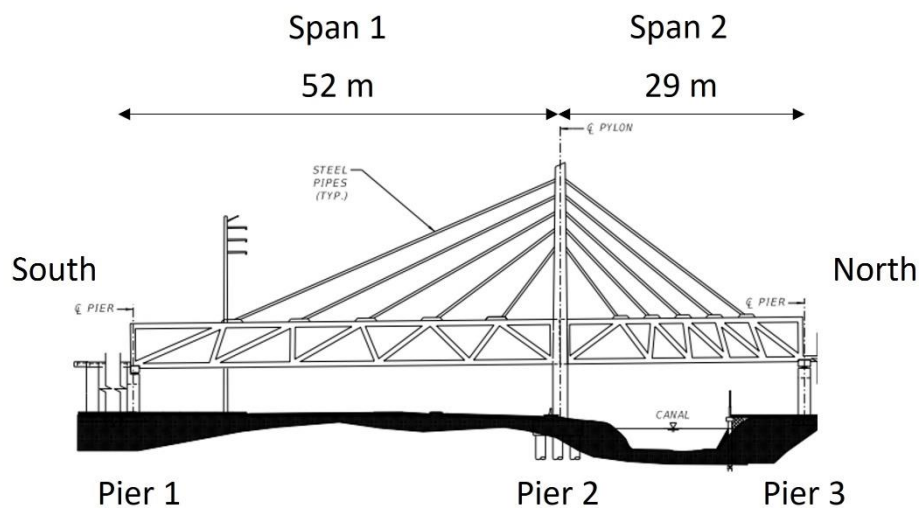

Figure 2: Longitudinal view, with piers highlighted [24].

The deck, 0.45 m thick and 9.60 m wide, is characterized by the presence of 12 longitudinal post-tensioned tendons (D1-D6) in span 1 while span 2 presents 6 longitudinal post-tensioned tendons (D7-D9). The tendons D7, D8 and D9 of the span 2 are located in the same position of the span 1 tendons D3, D4 and D5 but there are no tendons that continue along the length of both spans. Figs. 3 and 4 show the cross-section of the deck and the disposition of the post-tensioned tendons, respectively.
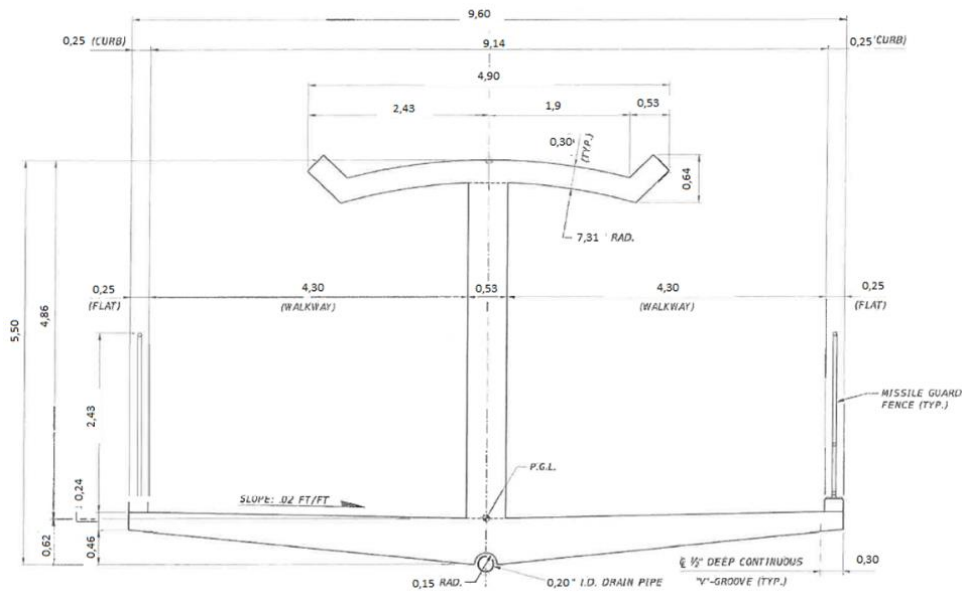
4

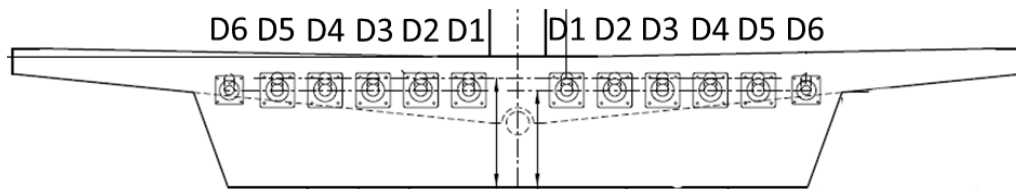Figure 3: Drawing of the deck cross-section (dimensions in meter) [24].

Figure 4: Drawing of the deck post-tensioned tendons [24].

In addition to the longitudinal post-tensioned tendons, 65 and 40 transverse post-tensioned tendons are presented in span 1 and 2. Table 2 summarizes the main characteristics of the post-tensioned tendons of the deck.

Table 2: Deck post-tensioned tendons main characteristics.

direction	name	span	number	dimension (n x Φ)	length	post-tensioned jacking force
[-]	[-]	[-]	[-]	[-]	[m]	[kN]
Longitudinal	D1	1	2	12 x 15.2 mm	52.8	2095
Longitudinal	D2	1	2	19 x 15.2 mm	52.8	3314
Longitudinal	D3	1	2	19 x 15.2 mm	52.8	3314
Longitudinal	D4	1	2	19 x 15.2 mm	52.8	3314
Longitudinal	D5	1	2	19 x 15.2 mm	52.8	3314
Longitudinal	D6	1	2	19 x 15.2 mm	52.8	3314
Longitudinal	D7	2	2	19 x 15.2 mm	30.1	3167
Longitudinal	D8	2	2	19 x 15.2 mm	30.1	3167
Longitudinal	D9	2	2	19 x 15.2 mm	30.1	3167
Transverse	-	1	65	4 x 15.2 mm	9.7	832
Transverse	-	2	40	4 x 15.2 mm	9.7	832

The canopy is characterized by a thickness equal to 0.30 m and by a width equal to 4.90 m. In this case, 8 post-tensioned tendons (C1-C4) have been used in span 1 while in span 2 other 6 post-tensioned tendons (C1, C4 and C5) are present. It possible to notice that tendons C1 and C4 are continuous along the two spans and the tendon C5 (span 2) is located in the same position of the

tendon C2 (span 1). The disposition of the canopy post-tensioned tendons is shown in Fig. 5 while Table 3 reports the related main characteristics.
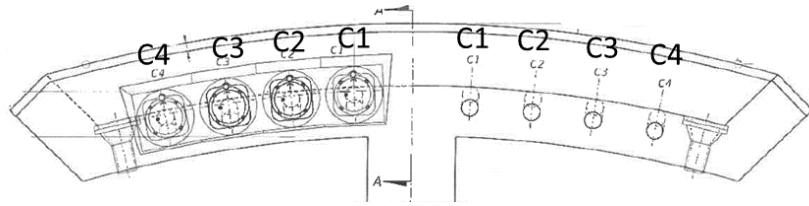

Figure 5: Drawingn of the canopy post-tensioned tendons [24].

Table 3: Canopy post-tensioned tendons main characteristics.

direction	name	span	number	dimension (n x Φ)	length	post-tensioned jacking force
[-]	[-]	[-]	[-]	[-]	[m]	[kN]
Longitudinal	C1	1-2	2	12 x 15.2 mm	82.9	2473
Longitudinal	C2	1	2	12 x 15.2 mm	52.8	2362
Longitudinal	C3	1	2	12 x 15.2 mm	52.8	2375
Longitudinal	C4	1-2	2	12 x 15.2 mm	82.9	2573
Longitudinal	C5	2	2	12 x 15.2 mm	30.1	2309

The concrete truss is made with 24 diagonal and vertical elements: 12 located in the span 1 and other 12 in span 2, which follow the external cables direction (Fig. 6).
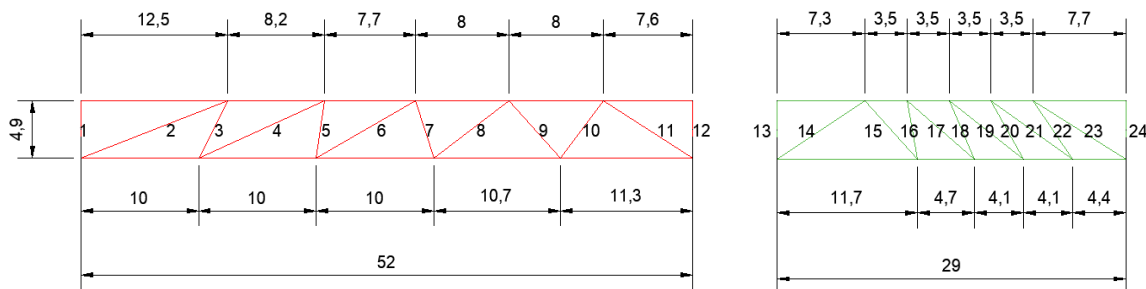

Figure 6: Span 1 (red) and span 2 (green) diagonal elements (dimensions in meters).

The diagonal elements are characterized by a rectangular section 0.53x0.61 m except for diagonal 2 which has dimensions 0.53x0.91 m. The vertical elements located at the far end of the truss have cross-section dimensions equal to 0.53x0.91 m while the other vertical elements present cross-section dimensions equal to 0.53x0.88 m. It can be noted that the elements 2, 3, 5, 6, 7, 8, 10, 11, 15, 16, 17, 18, 19, 20, 21, 22 and 23 are post-tensioned. Table 4 summarizes the main characteristics of the elements of the truss.

Table 4: Diagonal and vertical elements main characteristics.

name	cross-section dimension	longitudinal steel reinforcement	number post-tensioned rebars	diameter post-tensioned rebars	length	post-tensioned jacking force
[-]	[m]	[-]	[-]	[mm]	[m]	[kN]
1	0.53x0.91	14Φ36	-	-	-	-
2	0.53x0.91	12Φ25	2	45	13.0	1245
3	0.53x0.61	8Φ22	4	45	5.5	1245

4	0.53x0.61	10Φ22	-	-	-	-
5	0.53x0.61	8Φ22	2	35	5.3	735
6	0.53x0.61	8Φ22	2	45	10.6	1245
7	0.53x0.61	8Φ22	1	45	5.6	1245
8	0.53x0.61	8Φ22	4	45	8.9	1245
9	0.53x0.61	10Φ22	-	-	-	-
10	0.53x0.61	8Φ22	4	64	6.7	1730
11	0.53x0.61	8Φ22	2	45	10.0	1245
12	0.53x0.61	6Φ22 + 6Φ36	-	-	-	-
13	0.53x0.61	6Φ22 + 6Φ36	-	-	-	-
14	0.53x0.61	10Φ22	-	-	-	-
15	0.53x0.61	8Φ22	4	45	6.7	1068
16	0.53x0.61	8Φ22	1	35	5.3	632
17	0.53x0.61	8Φ22	4	35	7.4	735
18	0.53x0.61	8Φ22	1	35	5.4	530
19	0.53x0.61	8Φ22	2	35	7.8	735
20	0.53x0.61	8Φ22	1	35	5.6	632
21	0.53x0.61	8Φ22	2	35	8.3	530
22	0.53x0.61	8Φ22	2	35	5.8	735
23	0.53x0.61	8Φ22	2	35	8.6	530
24	0.53x0.61	14Φ36	-	-	-	-

As mentioned before, the bridge has been realized using Accelerated Bridge Construction method (ABC) [25], hypothesizing the following main phases:

1. construction of the piers 1 and 3 and of the pier 2 basement;
2. construction of the span 1 positioned on temporary supports in the bridge staging area. This phase is subdivided into several sub-steps: (i) construction of the deck, (ii) construction of the truss elements, (iii) construction of the canopy. Consequently, the interface between the vertical and diagonal elements of the truss with the deck and the canopy is represented by cold joints. Once the concrete has reached a compressive strength equal to 41 MPa, post-tensioning of the elements is carried out following this scheme: D1 longitudinal deck tendons, C2 longitudinal canopy tendons, diagonal elements 2 and 11 of the truss, D2-D3-D4-D5-D6 longitudinal deck tendons, transverse deck tendons, disassembly of the temporary supports, diagonal elements 3 and 10, diagonal elements 5 and 8 of the truss, diagonal elements 6 and 7 of the truss and C3 longitudinal canopy tendons. In the diagonal elements of the truss (except for the elements 2-11) bonded post-tensioning system has been applied;
3. positioning of the span 1 and application of post-tension at the longitudinal rebars of the pier 2. After this step, the post-tension applied to the diagonal elements 2 and 11 is removed;
4. construction of the span 2 considering the following sequence for the application of the post-tension in the structural elements: D7 longitudinal deck tendons, C5 longitudinal canopy tendons, diagonal elements 15 and 23 of the truss, diagonal elements 16 and 22 of the truss, diagonal elements 17 and 21 of the truss, diagonal elements 18 and 20 of the truss, diagonal element 19 of the truss, D8-D9 longitudinal deck tendons and transverse deck tendons;
5. bridge completed. Completion of pier 2 and positioning of external cables.

As reported in [26], the collapse of the bridge occurred at the end of the phase 3 on March 15, 2018 during its construction. In fact, at the end of February the presence of several cracks has been observed in correspondence to the node between the elements 11 and 12 (node 11, 12) after the post-tension remotion in the elements 2 and 11. Consequently, a new application of post-tension in element 11 has been considered (phase 3a). During the execution of this phase the bridge collapsed (Fig. 7). In

particular, it is important to highlight that the re-tensioning of the element 11 was not considered during the bridge design phase where the above-mentioned construction phases have been defined. In fact, the reapplication of the post-tension had increased the axial force of the diagonal element and consequently the shear action of the node. In addition, numerous contradictions were highlighted in the design report: the main problems were having underestimated the forces acting in the truss and having overestimated the resistance capacity of nodes 1, 2 - 2, 3 and 11, 12.

It can be assumed that the bridge has never been in safe conditions, mainly because the interface surface of the cold joints had not undergone any type of work and remained smooth, contrary to what the designers assumed in the design report. This happened probably because the necessary processing had not been accurately indicated in the design [26].
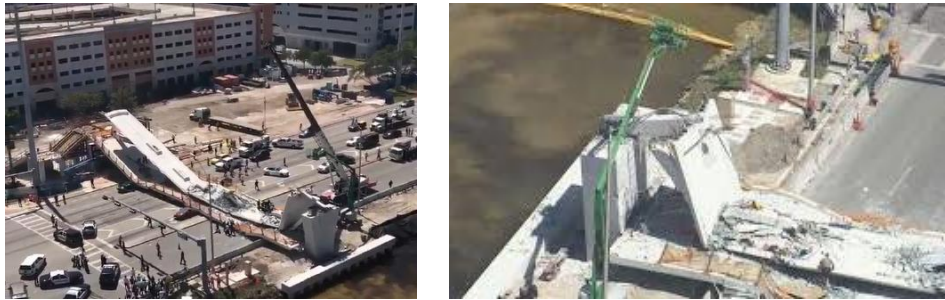

Figure 7: Collapse of the bridge.

3. Structural modelling and numerical analysis

To analyse the initiation of the failure mechanism of the pedestrian bridge during its construction, a Finite Element Model (FEM) has been implemented using MIDAS Gen [27] commercial software where the deck, the canopy and the elements of the truss have been modelled using Timoshenko beam elements, in order to reduce the computational effort (Fig. 8) [28-30]. The choice to implement the truss with beam elements has been made to be able to obtain the value of bending moments caused by the eccentric post-tensioning and to consider the joints between the different elements of the truss as fixed.

Construction Stage Analysis has been performed, considering the different phases described in previous Section 2, to analyse the evolution of the internal actions acting on the different structural elements during the construction process. All the construction phases were implemented changing the post-tensioning and the boundary conditions (Table 5). The loads considered during the analysis are (i) the self-weight of the structural elements and (ii) the post-tension. No live and temperature loads have been added to the bridge because the analysis wanted to understand the reason of the collapse during the construction process.
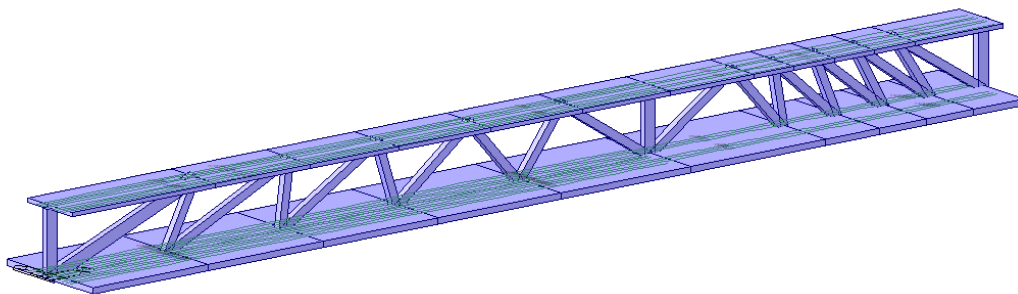

Figure 8: FEM of the RC bridge.

As mentioned before, the span 1 of the bridge was prefabricated off-site in the bridge staging area, following the ABC rules, with three different concrete casts: one for the deck, one for the truss and

one for the canopy, creating a discontinuity surface between them (cold joint). When the concrete reached a compressive strength equal to 41 MPa, the post-tension of the deck, canopy and truss elements has been applied; during this stage the span can be considered as a simple beam with pin ned boundaries (Fig. 9a). The second phase that was considered is the transportation phase, in which four SPTM were used to move the span: two of them were positioned in node 3, 4 and the other two in node 9, 10, creating cantilevered end (Fig. 9b). In the third phase, after transportation, the main span went back to a simple pinned truss and diagonal 2 and 11 were de-tensioned. In the fourth stage (called phase 3a, not foreseen in the design) the post-tension of diagonal 11 was reapplied, and this brings to the global collapse of the bridge. Finally, the whole bridge with both spans has been modelled, even though it has never been built, as a continuous beam (Fig. 9c).

Table 5: Construction phases (if grey post-tension is applied, if white post-tension is not applied).

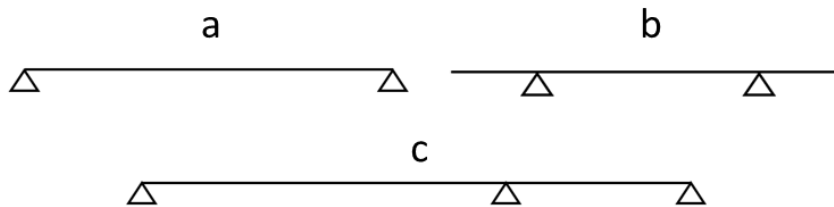| Name		Boundary conditions	Deck and canopy post-tension	Truss post-tension	Diagonal 2 post-tension	Diagonal 11 post-tension
Phase 1	Simple beam	Pinned (Figure 9a)	■	■	■	■
Phase 2	Transportation	Cantilevered ends (Figure 9b)	■	■	■	■
Phase 3	De-tensioning	Pinned (Figure 9a)	■	■		
Phase 3a	Re-tensiong 11	Pinned (Figure 9a)	■	■		■
Phase 5 (only numerical)	Complete bridge	Continuous beam (Figure 9c)	■	■		

Figure 9: (a) Simple pinned beam (phase 1, 3 and 3a); (b) beam with cantilevered end (phase 2); (c) continuous beam with 2 spans (phase 5).

In order to understand the causes which led to the bridge collapse, a comparison between the forces acting on the structural elements of the bridge during the analysed construction phases and their capacity has been carried out, following as reported in [31]. In particular, the analysis focuses on applying the checks on each truss element for all of the construction phases summarized in Table 5 and calculate the safety factor (SF) defined as reported in Eq.1:

$$SF = \frac{Capacity}{Load} \tag{1}$$

As mentioned before, the loads applied to the bridge are obtained considering the combination of the self-weight of the structural elements and of the post-tension acting on the structural elements (applied considering the sequence scheme described in previous Section 2) without any load multiplier. Also the elements capacity is evaluated without applying any reduction factor.

Considering the bending and axial force check, the results obtained show values of SF greater than 1 for all the analysed construction phases. In fact, the lower SF value calculated is equal to 1.32 for the truss diagonal element 12 in correspondence to the phases 1 and 3a. Also the shear check showed SF values always greater than 1. The lower SF value obtained is equal to 1.50 for the truss elements 1 and 12 in correspondence to the phases 1 and 3a.

On the contrary, the interface shear friction check is characterized by SF values less than 1. In this case, the interface shear transfer between two concrete cast at different times has been considered, using the relation reported in Eq. 2:

$$V_{ui} \leq \Phi V_{ni} \tag{2}$$

where V_{ui} is the interface shear force, V_{ni} is the nominal interface resistance and Φ is the shear resistance factor, in this case considered equal to 1. In particular, V_{ui} is calculated breaking down the axial force (N) acting on the structural element obtained from the construction stage analysis (Fig. 10) considering that the horizontal component is the shear force while the vertical component (P_c) is the normal force to the shear plane as shown in Eqs. 3-4 [31].

$$V_{ui} = N \cdot \sin \alpha \tag{3}$$

$$P_c = N \cdot \cos \alpha \tag{4}$$

In this case the structural elements have been considered as trusses, neglecting any shear components.
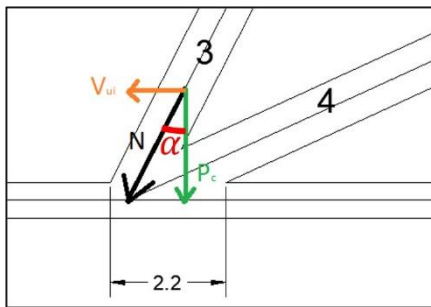
Element	Angle	Element	Angle
[-]	[°]	[-]	[°]
1	90	7	108
2	21	8	37
3	63	9	131
4	25	10	53
5	82	11	147
6	30	12	90

Figure 10: Breaking down of the axial force and inclination of the elements of the truss.

The nominal shear resistance of the interface plane (V_{ni}) is calculated as reported in Eq. 5:

$$V_{ni} = cA_{cv} + \mu(A_{vf}f_y + P_c) \tag{5}$$

This equation comes from a modified pure shear friction model. In fact, this relation assumes the resistance as directly proportional to the normal clamping force ($A_{vf}f_y + P_c$), obtained from the shear reinforcement area (A_{vf}), reported in Table 6, times the steel yield strength ($f_y = 415$ MPa) and the normal force (P_c, which is considered equal to 0 if tensile force) through a friction coefficient μ, plus a contribution (coming from experimental data) of the aggregate interlock (cA_{cv}), where A_{cv} is the area of concrete considered to be engaged in interface shear transfer and c is the cohesion.

Table 6: Elements of truss steel reinforcement.

Node	Rebar	Rebar cage			A_{PT}	A_{vf}
[-]	[mm^2]	[mm^2]			[mm^2]	[mm^2]
1,2	1921	4935	5Φ22	2Φ19	1140	7996
2,3	830	4536	6Φ19	2Φ19	6808	12175
3,4	785	7977	9Φ22	2Φ19	5668	14430
4,5	840	3969	5Φ19	2Φ19	1905	6715
5,6	824	5696	6Φ22	2Φ19	3496	10016
6,7	802	3969	5Φ19	2Φ19	3103	7875
7,8	859	5696	6Φ22	2Φ19	5341	11895
8,9	854	3969	5Φ19	2Φ19	3829	8652
9,10	963	5696	6Φ22	2Φ19	10277	16936
10,11	743	3969	5Φ19	2Φ19	12009	16721
11,12	8689	4175	4Φ22	2Φ19	1732	14597

Moreover, the resistance is defined by Eq. 6:

$$V_{ni} < \min (K_1 f_c A_{cv};\ K_2 A_{cv}) \tag{6}$$

These limits exist to prevent crushing or shearing of aggregate along the shear plane for the first and the second due to the lack in experimental data.

To evaluate the cohesion (c) and the friction factors (μ, K$_1$ and K$_2$) two different cases have been considered in this research work (Table 7): (i) normal-weight concrete places against a clean concrete surface with surface intentionally roughened to an amplitude of 6.35 mm and (ii) concrete place against a clean concrete surface, but not intentionally roughened [30].

Table 7: Cohesion and friction factors.

	c [MPa]	μ	K$_1$	K$_2$ [MPa]
1	1.65	1	0.25	10.34
2	0.52	0.6	0.20	5.52

Tables 8 and 9 summarize the results obtained for both cases although during the bridge construction the surface was left smooth.

Table 8: Shear friction check, case 1 (in bold SF less than 1.0).

Node	Phase 1		Phase 2		Phase 3		Phase 3a		Complete	
	V_{ni}	SF	V_{ni}	SF	V_{ni}	SF	V_{ni}	SF	V_{ni}	SF
	[kN]	[-]	[kN]	[-]	[kN]	[-]	[kN]	[-]	[kN]	[-]
1,2	9442.8	**0.96**	5822.1	10.81	8611.4	1.12	8611.4	1.12	7749.8	1.41
2,3	13161.2	1.22	13213.4	3.98	12273.7	1.43	12273.6	1.43	12239.3	1.79
3,4	11517.6	2.59	12056.4	2.15	11418.6	2.63	11418.6	2.63	11345.4	3.97
4,5	6155.2	1.79	6134.0	2.19	6147.3	1.82	6147.3	1.82	6138.0	3.85
5,6	7563.4	3.06	7776.0	3.28	7591.8	3.06	7594.8	3.05	7575.9	7.14
6,7	7358.5	3.72	7367.0	4.09	7362.6	3.71	7360.2	3.70	7389.6	53.42
7,8	9425.9	5.02	9425.9	5.35	9425.9	4.99	9425.9	5.02	9425.9	26.43
8,9	7507.9	8.58	7507.9	9.81	7507.9	8.27	7507.9	8.60	7507.9	6.42
9,10	9316.3	14.83	9316.3	2.69	9316.3	14.57	9316.3	14.83	9316.3	11.23
10,11	8055.9	1.72	8055.9	2.07	8055.9	3.00	8055.9	1.72	8055.9	1.78
11,12	5682.2	**0.83**	5628.2	5.42	5628.2	1.18	5628.2	**0.83**	5628.2	**0.94**

Table 9: Shear friction check, case 2 (in bold SF less than 1.0).

Node	Phase 1		Phase 2		Phase 3		Phase 3a		Complete	
	V_{ni}	SF	V_{ni}	SF	V_{ni}	SF	V_{ni}	SF	V_{ni}	SF
	[kN]	[-]	[kN]	[-]	[kN]	[-]	[kN]	[-]	[kN]	[-]
1,2	5087.5	**0.52**	2915.1	5.41	4588.7	**0.60**	4588.7	**0.60**	4071.7	**0.74**
2,3	7219.7	**0.67**	7251.0	2.18	6687.1	**0.78**	6687.1	**0.78**	6666.5	**0.98**
3,4	6362.5	1.43	6436.3	1.15	6303.1	1.45	6302.8	1.45	6259.2	2.19
4,5	3244.8	**0.94**	3232.0	1.15	3240.0	**0.96**	3240.3	**0.96**	3234.4	2.03
5,6	4039.8	1.68	4167.4	1.76	4056.9	1.63	4058.7	1.63	4047.3	3.81
6,7	4029.0	2.04	4034.1	2.24	4031.5	2.03	4030.0	2.03	4047.7	29.26
7,8	5032.0	2.68	5032.0	2.86	5032.0	2.66	5032.0	2.68	5032.0	14.11
8,9	4008.1	4.58	4008.1	5.23	4008.1	4.42	4008.1	4.59	4008.1	3.43
9,10	4873.5	7.91	4973.5	1.44	4973.5	7.78	4973.5	7.92	4973.5	5.99
10,11	4300.6	**0.92**	4300.6	1.10	4300.6	1.60	4300.6	**0.92**	4300.6	**0.95**
11,12	3004.6	**0.45**	3004.6	2.89	3004.6	**0.63**	3004.6	**0.45**	3004.6	**0.50**

For the case 1 only the nodes 1, 2 and 11, 12 are characterized by SF values less than 1. In fact, node 1, 2 presents a SF = 0.96 in correspondence to the phase 1 while node 11, 12 is characterized by SF values equal to 0.83, 0.83 and 0.94 during phase 1, phase 3a and once construction of the bridge is completed, respectively. Fig. 11 reports a synthesis of the above-commented results.

On the contrary, analysing the results obtained for the case 2, several nodes are characterized by SF values less than 1 as it is possible to see in Table 9 and Fig. 12. Also in this case, the most critical node is the 11,12 which presents the lowest values of the SF.
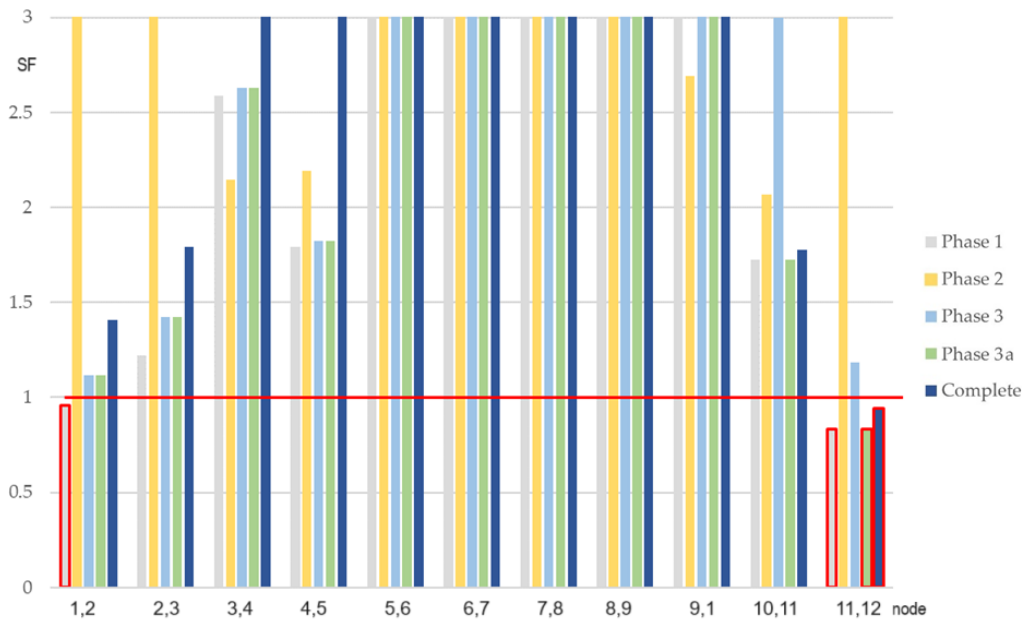

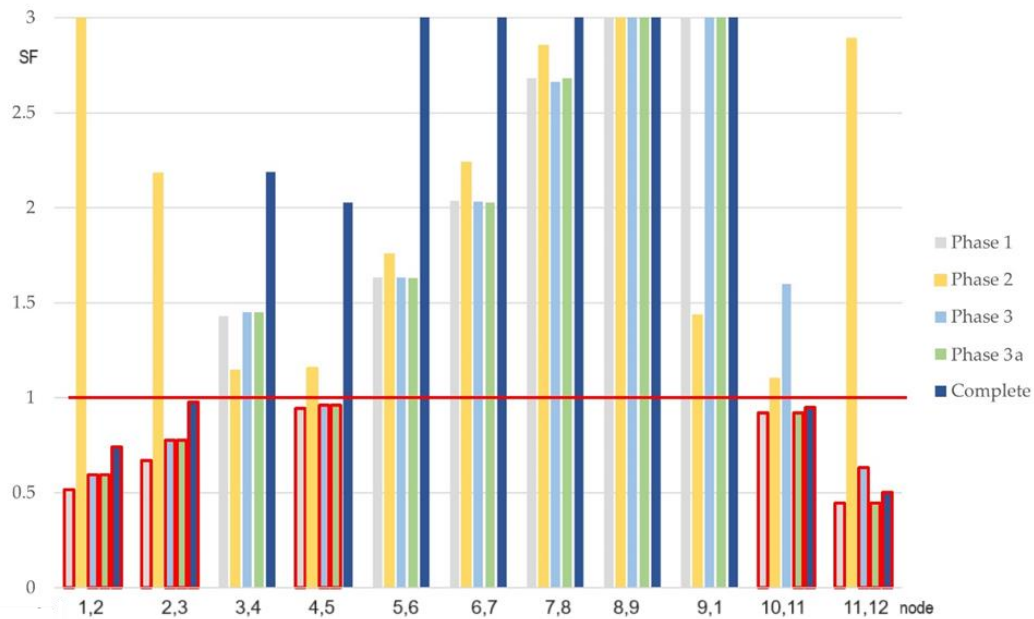Figure 11: SF values of the shear friction check, case 1.

Figure 12: SF values of the shear friction check, case 2.

To better understand the initiation of the failure mechanism occurs in node 11, 12 a detailed Finite Element Model has been implemented through MIDAS FEA NX commercial software [32] where the structural elements of the node 11, 12 are modelled using solid elements having maximum mesh size equal to 0.05 m (Fig. 13a). The two post tensioning bars (2Φ45) have been modelled as embedded trusses within the related structural element (Fig. 13b) as all of the longitudinal rebar and stirrups of the truss and the reinforcement cage of the node (Fig. 13c). Simple pinned beam condition was implemented in order to correctly reproduce the structural behaviour of the analysed node. Furthermore, a pinned connection has been realized under the deck, modelling a triangular prism to guarantee rotations; then on the right end and on the left end of the deck a roller with free vertical translation has been applied (Fig. 14a).

To reproduce the correct load conditions, self-weight (Fig. 14b) and post-tension have been applied using an appropriate function available in MIDAS FEA NX library. Moreover, elements axial force obtained from the previous analysis have been added as pressure load. (Fig. 14c).
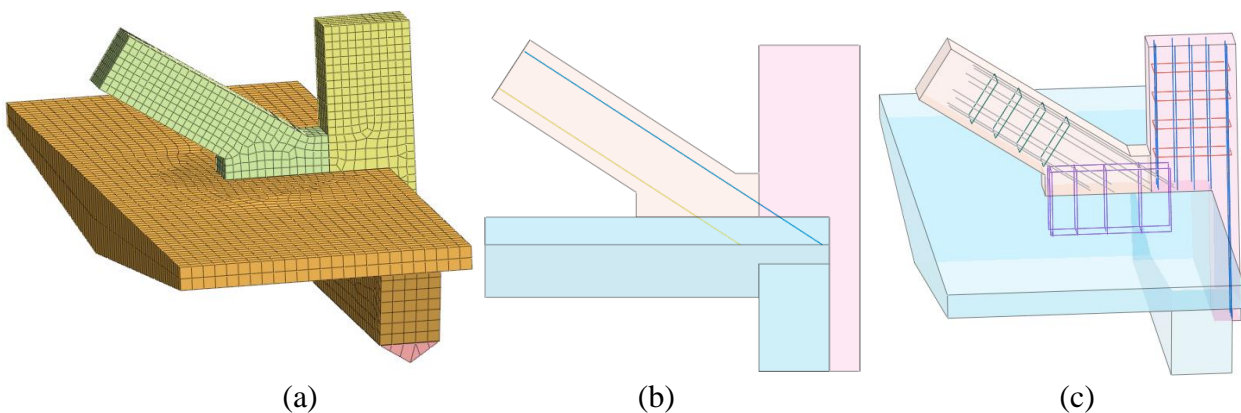

| (a) | (b) | (c) |

Figure 13: (a) FEM node 11-12; (b) post-tensioned bars in diagonal 11; (c) Rebar of the node 11-12.

(a)   (b)   (c)
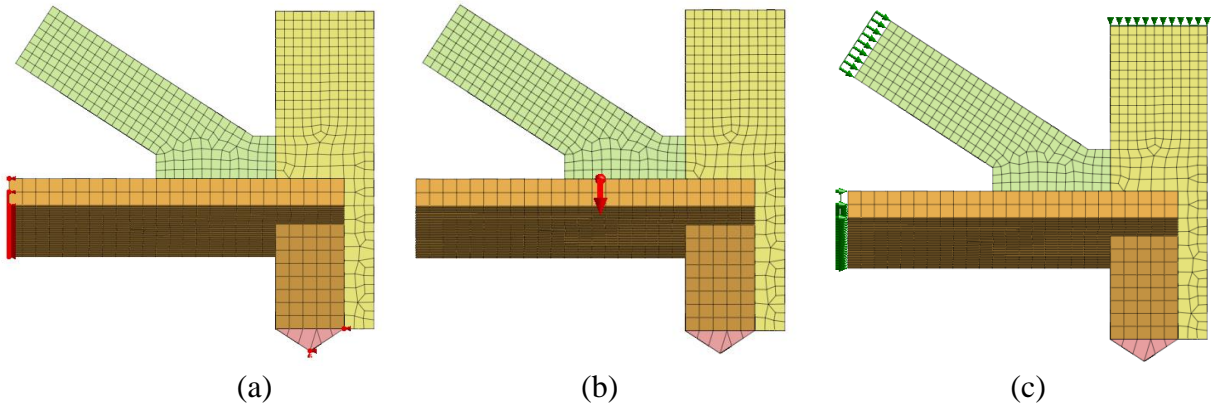
Figure 14: (a) Boundary conditions; (b) self-weight; (c) pressure load.

Construction stage analysis has been carried out considering the construction phases reported in Table 5. As reported in Table 1, the bridge was built using class VI concrete. Consequently, a compressive strength (f_c) equal to 58.60 MPa and a tensile strength (f_t) equal to 4.53 MPa has been considered.

The results show that a value of tensile stress equal to 6.78 MPa, acting in the area in correspondence to the node 11, 12 has been obtained considering the phase 1 (Fig. 15). However, during phase 3, when the element 11 is de-tensioned, the tensile stress lowers down to 5.44 MPa, improving the situation (Fig. 16). Taking into account the results obtained for the phase 3a, when the element 11 is re-tensioned in an eccentric way, the stresses go up to 8.71 MPa (Fig. 17), indicating the cracked concrete. Moreover, it is possible to notice that the position of the exceeded tensile stresses coincides with the cracks that were actually created (Figs. 18, 19).

Another important consideration is referred to the evolution of the stresses acting on the rebars of the node 11, 12, assuming that the concrete was cracked and only the rebars are able to resist to the forces acting in the node. The rebar shear cage in this node is composed by 2Φ19 and 8Φ22, having an area equal to 3608 mm^2. Table 10 summarizes the evolution of the stresses acting on the rebars of the node 11, 12. It is possible to notice that, during phase 3a the value of stresses is equal to 422 MPa, greater than the tensile yield strength of the ASTM A615 Grade 60 steel ($f_{y,60}$) as well for the shear stresses where already in phase 1 are higher than the resistance (755 MPa).

Once again, the conclusion is that the bridge collapsed because of a local problem, the node 11, 12 had a really low amount of rebar and re-tensioning member 11 caused the node to give in.
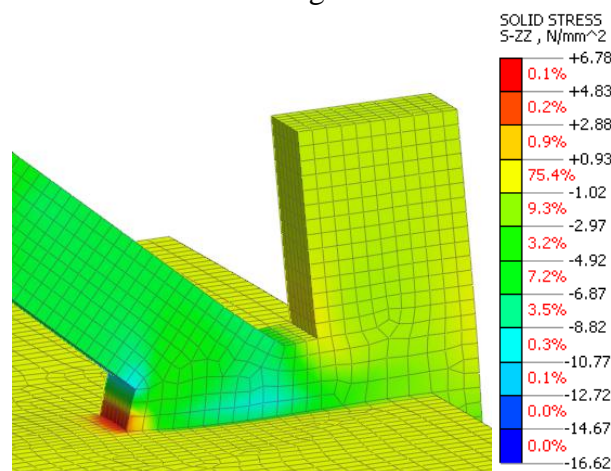

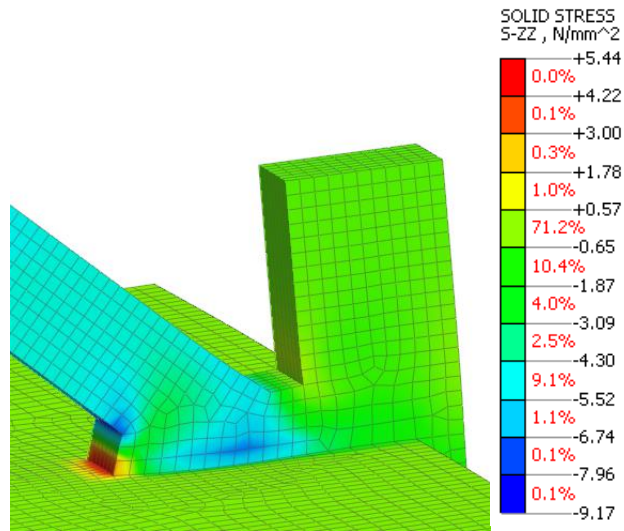Figure 15: Results of the phase 1.
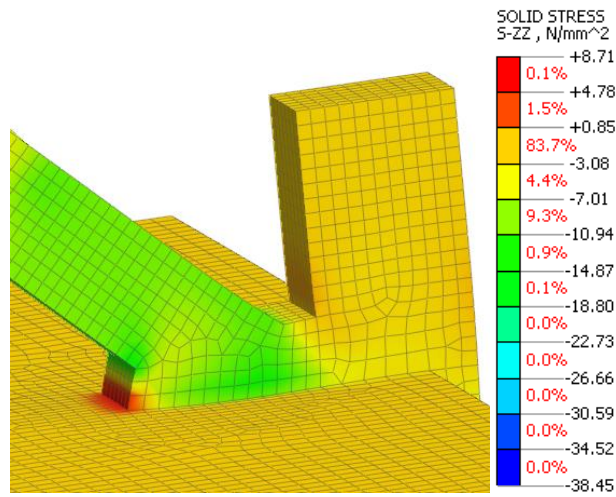
Figure 16: Results of the phase 3.

Figure 17: Results of the phase 3a.

Figure 18: Cracks in node 1, 2 after phase 1 (left) and cracks in node 11, 12 after phase 1 (right).
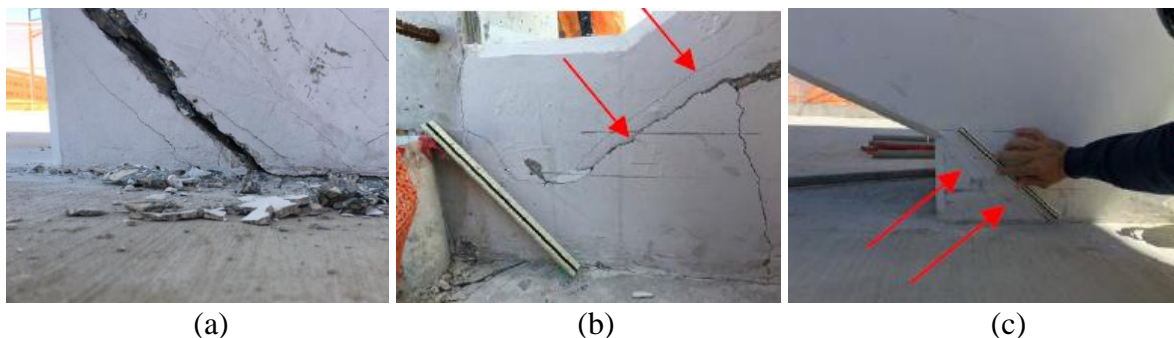
Figure 19: (a-b) Cracks in node 11, 12 after phase 3 and (c) cracks node 1, 2 after phase 3.

Table 10: Tensile and shear stresses acting on the rebar of the node 11, 12.

Phase	σ_{rebar}	$\tau_{yz,rebar}$
[n°]	[MPa]	[MPa]
1	346.67	755.56
2	20.29	124.60
3	295.45	539.07
3a	460.66	1010.50

4. Conclusions

In the paper, the failure mechanism occurred during the construction process of a post-tensioned reinforced concrete (RC) truss bridge, built using the Accelerated Bridge Construction (ABC) method has been investigated in detail, by means of several numerical analyses. A Finite Element Model (FEM) has been implemented where the deck, the canopy and the elements of the truss have been modelled using Timoshenko beam elements, in order to reduce the computational effort. Construction Stage Analysis has been carried out, to reproduce the construction process of the bridge in order to analyse the evolution of the internal actions acting on the different structural elements. A comparison between the forces acting on the structural elements of the bridge during the construction phases and their capacity has been carried out. Bending and axial force check showed safety factor (SF) values greater than 1 for all the analysed construction phases. Also, the shear check is characterized by SF values always greater than 1. On the contrary, for the interface shear friction check SF values less than 1 have been obtained. To perform this check two different cases have been analysed: the use of normal-weight concrete places against a clean concrete surface with surface intentionally roughened to an amplitude of 6.35 mm (case 1) and the use of concrete place against a clean concrete surface, but not intentionally roughened (case 2).

For case 1 only the nods 1, 2 and 11, 12 present SF values less than 1. In fact, node 1, 2 presents a SF = 0.96 in correspondence to the phase 1 while node 11, 12 is characterized by SF values equal to 0.83, 0.83 and 0.94 during phase 1, phase 3a and once construction of the bridge is completed, respectively. Considering the case 2, several nodes are characterized by SF values less than 1. Also in this case, the most critical node is the 11, 12 which presents the lowest values of the SF.

To better understand the collapse mechanism which occurs in node 11, 12 a Finite Element Model of the structural detail has been implemented by using solid elements. Construction stage analysis has been performed and the evolution of the stresses acting on the node have been obtained. Also in this case, it is possible to observe that the stresses acting on the node 11, 12 are greater than the resistant capacity of the considered structural elements and of the related node. In particular, appears evident that the collapse occurs during the re-tensioning phase of the truss element 11. In fact, the reapplication of the post-tension had increased the axial force on the diagonal and consequently the shear action on the node. The results obtained from the numerical analyses have been compared to

16

the crack patterns observed in the bridge before and after the collapse, finding a more than good match. On the consequence, it is possible to hypothesize that the bridge has never been in safe conditions due to the characteristics of the interface surface of the cold joints during its construction phases that were practically smooth, contrary to what the designers indicated in the design report.

According to as reported in [26], this research work has determined that the probable cause of the bridge collapse mechanism is due to errors in the structural design of the span 1 concrete truss elements 11 and 12 nodal region and in the related connection with the deck. However, the bridge failure occurred not only due to errors in the evaluation of acting loads and load-bearing capacity of the node 11, 12 but also for the incorrect realization of the roughness conditions of the interface surface of the cold joints.

Finally, it is important to highlight that in presence of non-symmetric concrete truss systems, the correct determination of construction details and construction phases is required in both the design and construction phases, in order to avoid the occurrence of possible collapses.

References

[1] Deng L, Wang W, Yu Y. State-of-the-art review on the causes and mechanisms of bridge collapse. Journal of Performance of Constructed Facilities 2016; 30(2): 04015005.

[2] Zhang G, Liu Y, Liu J, Lan S, Yang J. Causes and statistical characteristics of bridge failures: A review. Journal of Traffic and Transportation Engineering 2022; 9(3): 388-406.

[3] Xu FY, Zhang M, Wang L, Zhang JR. Recent highway bridge collapses in China: review and discussion. Journal of Performance of Constructed Facilities 2016; 30(5): 04016030.

[4] Fan Y, Zhu J, Pei J, Li Z, Wu Y. Analysis for Yangmingtan Bridge collapse. Engineering Failure Analysis 2015; 56: 20-27.

[5] Diaz EM, Moreno FN, Mohammadi J. Investigation of common causes of bridge collapse in Colombia. Practice Periodical on Structural Design and Construction 2009; 14(4).

[6] Cao R, El-Tawil S, Agrawal AK. Miami pedestrian bridge collapse: computational forensic analysis. Journal of Bridge Engineering 2020; 25(1): 04019121.

[7] Ozcelik M, Tutus O. An investigation on Botan Bridge (Siirt – Turkey) collapse during construction. Structures 2020; 25: 268-273.

[8] Tremblay M, Mitchell D. Collapse during construction of a precast girder bridge. Journal of Performance of Constructed Facilities 2006; 20(2).

[9] Choi HH, Lee SY, Choi IY, Cho HN, Mahadevan S. Reliability-based failure cause assessment of collapsed bridge during construction. Reliability Engineering & System Safety 2006; 91(6): 674-688.

[10] Tan JS, Elbaz K, Wang ZH, Shen JS, Chen J. Lessons learnt from bridge collapse: a view of sustainable management. Sustainability 2020, 12(3), 1205.

[11] Calvi GM. Moratti M, O'Reilly GJ, Scattarreggia N, Monteiro R, Malomo D, Calvi PM. Pinho R. Once upon a Time in Italy: The Tale of the Morandi Bridge. Structural Engineering International 2019; 29(2): 198-217.

[12] Scattarreggia N, Salomone R, Moratti M, Malomo D, Pinho R, Calvi GM. Collapse analysis of the multi-span reinforced concrete arch bridge of Caprigliola, Italy. Engineering Structures 2022; 251: 113375.

[13] De Domenico D, Messina D, Recupero A. Quality control and safety assessment of prestressed concrete bridge decks through combined field tests and numerical simulation. Structures 2022, 39: 1135-1157.

[14] Coni M, Mistretta F, Stochino F, Rombi J, Sassu M, Puppio ML. Fast falling weight deflectometer method for condition assessment of rc bridges. Applied Science 2021; 11(4): 1743.

[15] Jarek A, Dos Santos AT, Braganca MOGP, Pinkoski IM, Neri MAT, Diniz JHOT, Gomes RAN. Experimental and numerical investigations to evaluate the structural integrity of concrete beams exposed to an aggressive coastal environment. Structures 2022; 37(March): 795-806.

[16] Crespi P, Zucca M, Valente M, Longarini N. Influence of corrosion effects on the seismic capacity of existing RC bridges. Engineering Failure Analysis 2022; 140: 106546.

[17] Domaneschi M, Pellecchia C, De Iuliis E, Cimellara GP, Morgese M, Khalil AA, Ansari F. Collapse analysis of the Polcevera viaduct by the applied element method. Engineering Structures 2020; 214: 110659.

[18] Heng K, Li R, Li Z, Wu H. Dynamic responses of highway bridge subjected to heavy truck impact. Engineering structures 2021; 232: 111828.

[19] Design build team MCM-FIGG, Proposal for the BT-904 | FIU: University city prosperity project, 2015.

[20] Florida Department of Transportation, Standard Specifications for road and bridge construction, 2022.

[21] ASTM A615, Standard Specification for Deformed and Plain Carbon-Steel Bars for Concrete Reinforcement, 2022.

[22] ASTM A722, Standard Specification for High-Strength Steel Bars for Prestressed Concrete, 2021.

[23] ASTM A416, Standard Specification for Low-Relaxation, Seven-Wire Steel Strand for Prestressed Concrete, 2021.

[24] FIGG, FIU Bridge Construction Plans, 2016.

[25] Federal Highway Administration, Accelerated Bridge Construction. www.fhwa.dot.gov/bridge/abc/.

[26] National Transportation Safety Board, Accident Report NTSB/HAR-19/02 PB2019-101363. https://www.ntsb.gov/investigations/AccidentReports/Reports/HAR1902.pdf.

[27] MIDAS Gen, Analysis Reference, 2022.

[28] Zucca M, Reccia E, Longarini N, Eremeyev V, Crespi P. On the structural behaviour of existing RC bridges subjected to corrosion effects: Numerical insight. Engineering Failure Analysis 2023; 152: 107500.

[29] Zhou H, Chen S, Du Y, Lin Z, Liang X, Liu J, Xing F. Field test of a reinforced concrete bridge under marine environmental corrosion. Engineering Failure Analysis 2020; 115: 104669.

[30] Dong Z, Sun Z, Wu S, Tong F, Wang D. Influence of soil liquefaction effect on seismic failure mechanism of river-crossing simply-supported girder bridges subjected to near-fault ground motions. Engineering Failure Analysis 2023; 154: 107664.

[31] AASHTO LRFD Bridge Design Specifications, 9th Edition, 2021.

[32] MIDAS FEA, Analysis Reference, 2022.